ADVANCED MATERIALS INTERFACES
Open Access
www.advmatinterfaces.de

Underwater Acoustic Camouflage by Wettability Transition on Laser Textured Superhydrophobic Metasurfaces

Francesco P. Mezzapesa, Caterina Gaudiuso, Annalisa Volpe, Antonio Ancona, Salvatore Mauro, and Silvano Buogo*

The superhydrophobicity of submerged surfaces typically pertains to the trapped air film at the liquid–solid interface, subject to wettability transitions from a Cassie–Baxter state to more unstable states that gradually collapse to high retention regimes, which are energetically more favorable. In this work, the dynamic evolution of those transient metastable states is correlated to the underwater acoustic performance of laser textured superhydrophobic surfaces, resolving the dependence of the ultrasound spectral response with the immersion time to capture the genuine contribution of the hierarchical subwavelength morphology, regardless of the air layer effects. Acoustic wave attenuation of the incident ultrasound energy is extensively quantified in transmission, accounting for instantaneous broadband sound blocking (>30 dB) within the spectral range 0.5–1.5 MHz. As a result of the air layer detachment with the immersion time, transmission coefficients increase accordingly, while acoustic fields in reflection unexpectedly evolve toward stealthiness and naïve acoustic camouflage, mostly ascribable to dissipative mechanisms at air layer interfaces. The intrinsic decay of the air layer effect is tentatively determined at different frequencies, since quantitative understanding of the transient lifetime governing underwater surface wettability is critical to design stable superhydrophobic character of laser induced subwavelength metastructures on the most promising acoustic materials – from eco-friendly natural to artificial.

1. Introduction

In underwater acoustics, leveraging metasurfaces, that is, 2D equivalent of bulk metamaterials exhibiting inherently subwavelength building blocks, to develop unconventional functionalities for sound wave manipulation and control[1–4] is experiencing a tremendous impact on various fields, including underwater acoustic communication,[5] holographic rendering,[6,7] camouflage and invisibility cloaking,[8–10] de-noising and super-resolution sensing.[11] Engineering acoustic metasurfaces to condition the incident wavefront interacting with the subwavelength unit cells in water, yields to selective modulation of phase and amplitude of acoustic fields in reflection/transmission, which enables intriguing applications in multiple wave manipulation functions, including guiding and steering acoustic waves, enhancing underwater stealth and/or detection sensitivity, generating focused acoustic beams, switching on/off acoustic energy flow.[12–18]

In literature, it has already reported that modulating the surface topography of materials significantly affects their interaction with acoustic waves. Li et al.[19] investigated the acoustic response of aluminum plates structured by 1D Fibonacci array of rectangular ridges and compared the outcome in case of negative (from the smooth side) and positive (from the structured side) incidence of the acoustic wave. The transmission was significantly different in the whole range from 350 to 630 kHz (transmission ≈79% in case of positive incidence at a very visible peak @ 475 kHz, while an almost flat 10% transmission was observed for negative incidence). Bok et al.[20] found that creating a metasurface by using membranes and air-filled cavities resulted in increasing the sound transmission of ≈30% at the interface with water, despite only 0.1% of the acoustic energy was expected to be transmitted at 700 Hz. Feng et al.[21,22] exploited laser surface engineering to create a micro-patterned morphology on synthetic polymers reinforced with metals and compared the underwater acoustic response of the laser treated samples to the pristine. They claimed that, at the immersion in water, over 88% of the acoustic power incident on the textured surfaces was absorbed from 50 - to 250 kHz, as ascribed

F. P. Mezzapesa, C. Gaudiuso, A. Volpe, A. Ancona
Institute for Photonics and Nanotechnologies (IFN)
National Research Council (CNR)
Via G. Amendola 173, Bari 70125, Italy
E-mail: francescopaolo.mezzapesa@cnr.it
A. Volpe, A. Ancona
Intercollegiate Department of Physics "M. Merlin"
University of Bari and Polytechnic University of Bari
Via G. Amendola 173, Bari 70125, Italy
S. Mauro, S. Buogo
Institute of Marine Engineering (INM)
National Research Council (CNR)
Via di Vallerano, 139, Roma 00128, Italy

The ORCID identification number(s) for the author(s) of this article can be found under https://doi.org/10.1002/admi.202400124

DOI: 10.1002/admi.202400124

to the air plastron trapped into the artificial topography and the specimen's superhydrophobic behavior. However, after 2 h in the water, the air plastron dissolution at the liquid-solid interface caused the absorption to decrease (down to 3–7%). While this investigation gave some insight into the unstable behavior of superhydrophobic surfaces in terms of acoustic response, no relevant studies highlighting the underwater acoustic tunability induced by wetting transitions on metasurfaces are published, yet.

In this work, we fill this gap by exploring the dynamical evolution, from acoustic stealth to spectral selective enhanced visibility (acoustic camouflage), of the ultrasound response of laser surface textured aluminum specimen in the frequency range from 0.5 to 1.5 MHz, in terms of transmitted and reflected fields, with potential applications in underwater acoustic sensing and medical ultrasonic devices.

2. Experimental Section

2.1. Femtosecond Laser Surface Functionalization

Laser surface sculpting is known to be by far the most sustainable fabrication method to modify the wetting response of pure metallic substrates,[23,24] as neither specific chemicals nor waste are involved to confer an extra-ordinary superhydrophobicicity to the surface, for instance by generating nanoparticles decorating Laser-Induced Periodic Surface Structure (LIPSS), or direct laser writing of microfeatures, and/or a combination of both. However, textured surfaces are generally superhydrophilic right after the laser treatment, and their wetting response shifts to a stable hydrophobic or superhydrophobic character, depending on the multi-scale topography induced by optimizing the laser irradiation process. Among common metals, aluminum was shown to exhibit tailored superhydrophobic character when directly irradiated with femtosecond laser pulses,[25] and the wetting response was also correlated to hierarchical morphologies and combined effects of ripples and nanoparticles upon the textured surface.[26]

In this work, artificial periodic textures were generated on flat AA2024 specimen by means of a Pharos 1.5-SP laser from Light Conversion, emitting 200-fs (FWHM) horizontally polarized pulses at 1030 nm of central wavelength. The laser beam diameter focused on the sample surface was (19.6 ± 0.5) µm (1 e^{-2} peak intensity), measured with a CCD camera (FireWire BeamPro Model 2523 by Photon Inc.). The pulse energy was carefully set at 1 J cm^{-2} by placing a half waveplate followed by a polarizer right before a galvo-scanner (SCANLAB's IntelliSCAN 14) equipped with a 100 mm focal length F-Theta telecentric lens. Laser surface structuring was carried out in ambient air by overlapping, on the aluminum target, cross scanning patterns to generate periodic square-shaped structures separated by a hatch of 125 µm, followed by a 45° square-shaped pattern to finalize the aimed surface geometry.[27] The laser repetition rate was set at 200 kHz to ensure high processing speed (100 mm s^{-1}) over the (40 × 40 × 0.5) mm^3 scanned area. After fs-laser surface treatment, the textured samples were kept at (120 ± 1) °C for 3 h to accelerate the transition from hydrophilicity to hydrophobicity and to confer a stable wetting response in air.[28,29]

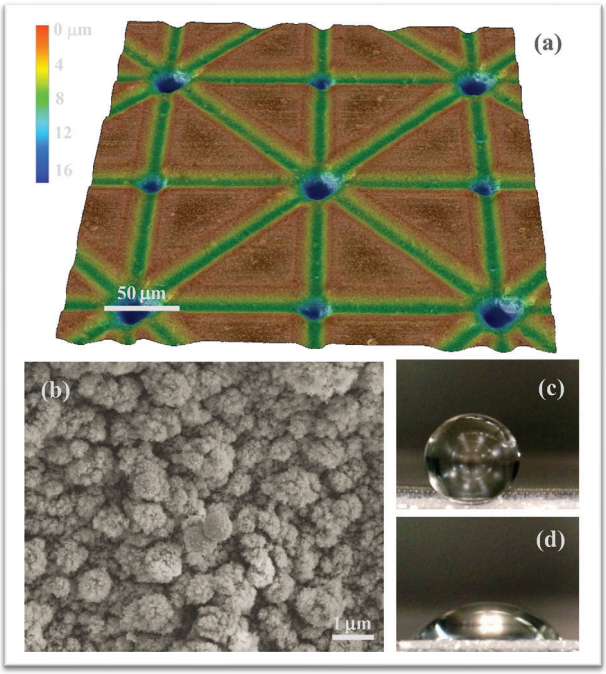

Figure 1. a) Representative 3D topography of AA2024 laser-textured surface by a digital microscope Keyence VHX, featuring triangular lattice[27] with a textured surface percentage above 70%. b) Sub-micron investigation of the hierarchical morphology by Σigma scanning electron microscopy (SEM) from Zeiss. Surface wetting response of c) superhydrophobic (CA ≥ 150°) and d) untextured (CA = 65 ± 1°) thermal treated specimen, respectively.

2.2. Surface Characterization

Figure 1a shows a representative 3D topography of the laser treated AA2024 surface, featuring periodic patterns with microgrooves of (8.3 ± 0.1) µm depth, which are expected to favor acoustic surface wave propagation (i.e., standing waveguide modes) and effective coupling in underwater sound absorbers, as predicted by the De Bruijn theory.[30]

In Figure 1b, higher resolution investigations by Σigma scanning electron microscopy (SEM) reveal a multi-scale morphology, with a hierarchical decoration of sub-micron bulges and pores, generally related to thermal effects (melting), which is known to initiate and influence the air layer effect on submerged superhydrophobic surfaces, as predicted by the Cassie–Baxter theory.[31] To characterize the surface wetting response in air, static contact angle (CA) measurements on the laser structured surfaces – after the thermal aging treatment, were conducted on three different spots using a digital goniometer, consisting of a Dino-lite portable microscope combined with a cold light lamp for backlighting of the drop (10 µL bidistilled water). The CA measurements were performed at ambient temperature (≈22.5 °C) and before water droplet deposition, the relative humidity was constantly monitored (68% RH). Figure 1c shows a superhydrophobic behavior of the textured surfaces, which could be explained by a change in surface chemistry (i.e., a higher concentration of carbon organic molecules responsible for low surface energy[25]), as confirmed by X-ray photoelectron spectroscopy (XPS) carried

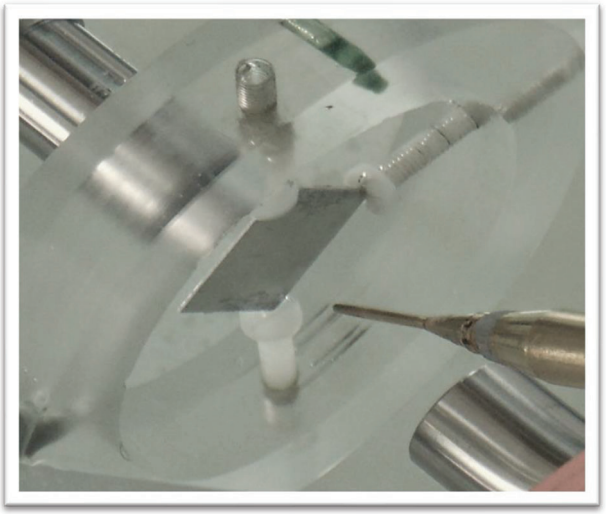

Figure 2. Schematic of the experimental setup for acoustic properties measurements in water, showing transmitting transducer and needle hydrophone (bottom right) and receiving transducer (up left), respectively. The sample (center) is mounted in its place using a ring-shaped holder with 55 mm internal diameter (to minimize edge diffraction effects and ensure proper surface orientation), with the superhydrophobic surface facing the source at a distance of 20 mm. The frequency range is purposely chosen between 500 kHz and 1.5 MHz (corresponding to a wavelength range between ≈1 and 3 mm in water) to maximize signal-to-noise ratio according to the transducers frequency response: specifically, the needle receive response at 45° is less than 3 dB down with respect to normal incidence. Transmitted and reflected wave signals are simultaneously acquired and averaged (n = 128) by a digital oscilloscope (not shown), and their RMS values are computed in separate time gates centered in the flat portion of each acoustic pulse. Before starting data collection, direct signals with no sample in place are repeatedly recorded until fluctuations, mostly due to reaching thermal equilibrium, are reduced to less than 1%.

out by Cardoso et al.[26] on AA2024 surfaces textured with similar laser process conditions. The untextured thermal treated sample was also characterized for comparison, as shown in Figure 1d.

2.3. Underwater Ultrasonic Measurement

A schematic of the experimental setup for underwater ultrasonic measurements of transmitted and reflected waves is shown in **Figure 2**. The overall system includes two ultrasonic piezoelectric transducers (Panametrics A303R and V303, used as source and receiver respectively) both with 1 MHz resonant frequency and 0.5″ diameter flat surface (unfocussed), and a 0.5 mm diameter PVDF (polyvinylidene fluoride) needle hydrophone (mod. NH0500 by Precision Acoustics Ltd.), immersed in a $(0.5 \times 0.2 \times 0.2)$ m^3 tank filled with distilled water, whose temperature is set at (25 ± 1) °C and constantly monitored. The transducers are mounted facing each other at approximately half depth with their axis aligned, to generate and record orthogonally incident and transmitted waves in the frequency range 0.5–1.5 MHz. The needle hydrophone is placed on the same side of the source with its axis oriented at 45° and the tip lying on the transducer axis, to record the wave reflected orthogonally by the sample with minimal interference on the incident wave. The ultrasonic source converts a train of 12 µs duration sinusoidal pulses, with 100 Hz

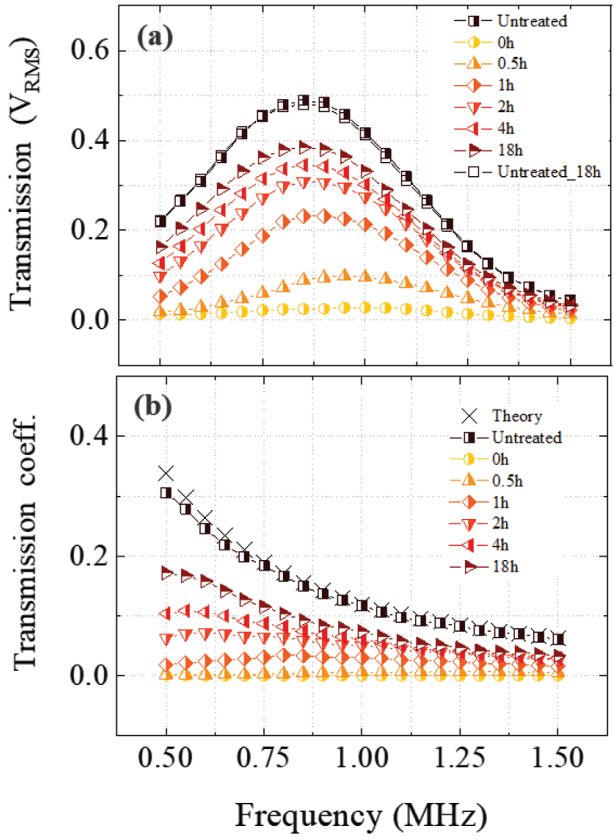

Figure 3. Underwater evolution of a) transmission signals and b) transmission coefficients for untreated and laser textured superhydrophobic aluminum foil with immersion time, respectively. The transmission coefficient curve of the pristine sample fits well with theoretical transmission coefficients, as calculated by Equations 1. Error bars are smaller than the symbol size. The acoustic impedance value in aluminum is 17.33 MRayl[19] and thin-layer approximation for sound wave transmission measurements is applied, the thickness of the specimen being an order of magnitude below the incident wavelength – ranging from 4.16 to 12.48 mm in aluminum.

repetition rate, into an acoustic incident wave, which is in turn reflected and transmitted by the sample placed between the hydrophone and the receiving transducer, respectively. The superhydrophobic (SH) surface of the specimen faces the source at a distance of 20 mm, and both the hydrophone and the detector are set at a distance of 10 mm from the specimen in order to separate direct transmitted and reflected signals from multiple reflections between sample and transducers.

3. Performance for Blocking Sound: Theory and Experiment

In order to infer the surface wettability effect on the underwater acoustic performance of the laser-treated superhydrophobic metasurfaces, we have investigated the time-evolution of the transmitted energy at a given frequency range and condition. **Figure 3a** shows the RMS transmitted signals through the untreated aluminum foil kept continuously immersed in water for 18 h, in order to compare it to the acoustic response of the

laser-treated counterpart. Noteworthy, less than 2% fluctuations in transmitted signals are registered on untreated samples throughout the experiments, here regarded as a benchmark for the setup long-term stability and accuracy. Besides, the time dependence of underwater transmission coefficients, as determined by the ratio of the squared transmitted sound intensity through the aluminum foil ($|V_{RMS}|^2$) to the incident sound intensity, is depicted in Figure 3b. The transmission coefficient curve of normal incident ultrasonic waves to a pristine sample (i.e., untreated) is also reported for comparison, which fits well with theoretical transmission coefficients,[21] as calculated by Equation (1):

$$T = \frac{4}{4cos^2 kD + \left(R_{12} + R_{21}\right)^2 \sin^2 kD} \quad (1)$$

where D is the thickness of the specimen, R_{12} (R_{21}) is the ratio of the acoustic impedance value of the acoustic wave in the aluminum (water) to the acoustic impedance value of the acoustic wave in the water (aluminum), k is the wave number. Interestingly, the laser treated specimen fresh of immersion in water (i.e., at 0 h) retains null values of transmission coefficients throughout the ultrasound frequency range under test, thus exhibiting broadband sound blocking operation owing to its inherent superhydrophobicity: the air layer trapped in the hierarchical micro-nanostructures at the surface is known to increase the apparent characteristic impedance and affect the instantaneous acoustic response of the submerged metallic metasurface. Moreover, the spectral analysis of transmission coefficients displays an increasing trend with the immersion time, as expected,[21] and proves experimental evidence of strong correlation between time-varying ultrasound insulation and air layer dissolution atop the laser-ablated metasurface. Hence, we demonstrate a fine methodology to monitor changes in dynamic wetting transition – from Cassie–Baxter to Wenzel state, causing transmission coefficients to progressively approach their saturation values as a result of air bubble detachment and diffusion into the surrounding water. Those saturation transmission coefficients, spanning from 63% (@1 MHz) to ≈54% (@1.5 MHz) of the corresponding pristine (i.e., untreated) value after almost one day of immersion, are homogenously attained over the entire spectral range under test and mostly ascribable to genuine dissipation/scattering of sound fields by the laser induced morphology at the surface only, as acoustic coupling among deep and interconnected micro-grooves is known to affect the acoustic wave attenuation in water.[32,33]

In **Figure 4** we use the loss function expressed in dB to quantify changes in underwater sound intensity with respect to the power carried by the incident waves and compare the dynamical evolution of acoustic fields both in transmission and reflection, respectively.

Specifically, the reflected sound waves are collected by placing the needle hydrophone at 45° from the perpendicular to the superhydrophobic surface of the specimen, as depicted in Figure 2. The superhydrophobic character of the surface wettability produces high acoustic energy dissipation in transmission soon after the immersion in water, albeit the reflected acoustic signals being almost preserved over the frequency range under test (see curves 0 h in Figure 4). This is predicted by the Cassie–Baxter wetting theory, the superhydrophobic surface performing as an

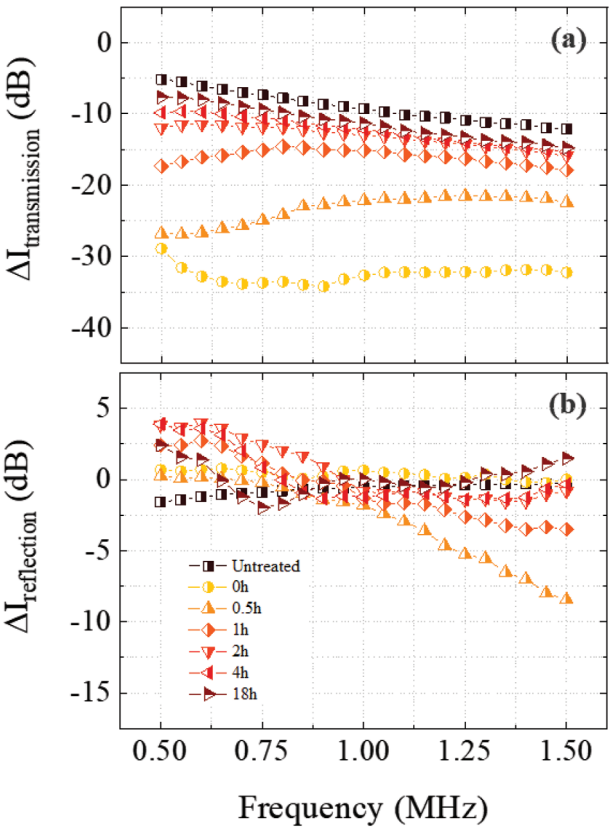

Figure 4. Comparison of underwater energy evolution both in a) transmission and b) reflection signals respectively, from untreated and superhydrophobic surfaces, at various immersion time. Error bars are smaller than the symbol size.

effective insulating structure when initially immersed underwater, along with the air layer at the liquid/solid interface making a replica of the laser textured micro-array, so as not to affect the reflection signals.[31]

Furthermore, in the time taken by the ultrasound transmitted energy through the metasurface to monotonically approach the reference value and finally saturate at a plateau value of ≈–2 dB to pristine (untreated), the dynamical evolution of acoustic fields in reflection changes dramatically. Intriguingly, the reflection energy is rapidly dissipated after the superhydrophobic surface is immersed in water for 30 min only, displaying a behavior going to stealth above 1 MHz and descending to −7.5 dB with respect to the pristine values at 1.5 MHz.

Conversely, reflection loss functions switching to a rather opposite trend occur at time > 1 h, as shown in Figure 4b, with laser treated surfaces happening to boost the acoustic field of reflected waves at low frequency with respect to untreated surfaces, the maximum acoustic visibility holding to + 5.5 dB at 0.5 MHz for few hours of immersion. Hence, unexpected inhomogeneities are disclosed by spectral analysis of the ultrasound fields reflected/transmitted by the laser textured specimen immersed in water, as highlighted in **Figure 5**.

Notably, an initial drop in acoustic reflected fields is shown in Figure 5b, more prominent at a frequency higher than 1 MHz, owing to the scattering of sound waves at liquid/air/solid

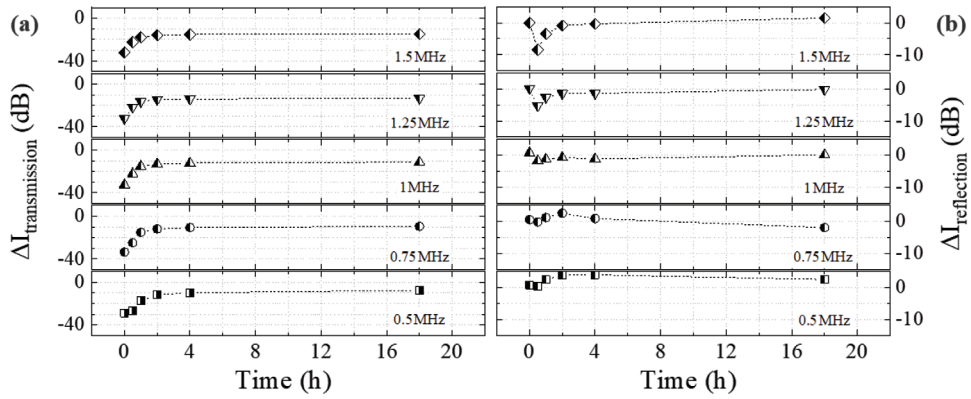

Figure 5. Underwater dynamical evolution of acoustic fields by superhydrophobic surfaces both in a) transmission and b) reflection, respectively. Error bars are smaller than the symbol size.

interfaces. We suppose that such an uneven energy dissipation, arising from the unique combination of surface morphology and wettability transition, may provide information about the actual thickness of the air layer and its degree of dissolution in water. Based on the evidence, the medium of acoustic waves, being water or air layer at the interface between water and superhydrophobic metasurfaces, plays a crucial role in governing the underwater acoustic performance at a given frequency range and condition. Nevertheless, the multi-scale hierarchical morphology of fs-laser textured metastructures (i.e., groove periodicity, geometry, depth, and width) is thought to genuinely affect the transmission and reflection field of sound waves in water, as long as enough time is left since the first immersion. The strategy to optimize the novel design of surface micro-nanomorphology and wetting response would require extensive further research that is beyond the scope of this paper.

4. Conclusion

In this work, we demonstrated that underwater ultrasound performances of submersed aluminum foils with laser textured metasurfaces may be heavily affected by their wetting properties. Analyzing the time history of the acoustic response upon immersion in the whole frequency range spanning from 500 kHz to 1.5 MHz, we unveiled a peculiar spectral dependence of the incident ultrasound wavefront interacting with the subwavelength microstructures on the surface, yielding to selective modulation of the acoustic field amplitude both in transmission and in reflection. In transmission, the laser treatment resulted in a broadband sound blocking behavior (>30 dB) occurring at the immersion. This behavior was ascribed to the air layer initially trapped in those multi-scale hierarchical structures and conferring a superhydrophobic response to the surface (Cassie–Baxter regime). However, the energy carried by the transmitted sound waves would monotonically approach untreated values after many hours in water, due to water filling at the protrusions of the artificial topography which almost perfectly restored the response of the untextured reference (transition to Wenzel state). In reflection, the apparent acoustic impedance of laser treated metastructures caused selective stealth regimes to be disclosed at the immersion. Noteworthy, naïve acoustic camouflage effects would progressively emerge in the entire spectral range investigated: those spectral modulations and the prominent drop above 1 MHz were likely due to multiple scattering and absorption mechanisms at the liquid/solid interface, where the air-layer was trapped. Such an uneven energy dissipation, yielded by unique combination of surface morphology and time-dependent transition of the wettability state, may unveil a peculiar correlation with the actual thickness of the air-layer and its degree of dissolution in water.

The results of this work will be the basis for the exploration of complex surface morphologies with a more stable/durable submersed wetting character, thus bringing innovation in underwater applications where robust control of acoustic response of lightweight materials, from metals to polymer and composite substrates, is highly attractive.

Conflict of Interest

The authors declare no conflict of interest.

Author Contributions

M.F.P. performed conceptualization, methodology, validation, data curation, visualization, wrote the original draft, and reviewed and edited the final manuscript; G.C. methodology, validation, data curation, wrote the original draft, and reviewed and edited the final manuscript; V.A. performed methodology, validation, data curation, and reviewed and edited the final manuscript; A.A. helped in fund raising, reviewed and edited the final manuscript; M.S. performed ultrasound measurement design, and reviewed and edited the final manuscript; B.S. performed ultrasound measurement design and execution, and reviewed and edited the final manuscript. M.F.P. thanks Pietro Paolo Calabrese and Alessandro Bini for their technical support.

Data Availability Statement

The data that support the findings of this study are available on request from the corresponding author. The data are not publicly available due to privacy or ethical restrictions.

Keywords

superhydrophobicity, surface functionalization, ultrafast laser texturing, underwater acoustics, wettability transition

Received: February 9, 2024
Revised: March 30, 2024
Published online:

[1] S. A. Cummer, J. Christensen, A. Alu, *Nat. Rev. Mater.* **2016**, *1*, 16001.
[2] G. C. Ma, P. Sheng, *Sci. Adv.* **2016**, *2*, 1501595.
[3] H. Ge, M. Yang, C. Ma, M. H. Lu, Y. F. Chen, N. Fang, P. Sheng, *Natl Sci Rev* **2018**, *5*, 159.
[4] B. Assouar, B. Liang, Y. Wu, Y. Li, J.-C. Cheng, Y. Jing, *Nat Rev Mater* **2018**, *3*, 460.
[5] X. Jiang, B. Liang, J. C. Cheng, C. W. Qiu, *Adv. Mater.* **2018**, *30*, 1800257.
[6] Y. B. Xie, C. Shen, W. Q. Wang, J. F. Li, D. J. Suo, B. I. Popa, Y. Jing, S. A. Cummer, *Sci. Rep.* **2016**, *6*, 35437.
[7] Y. F. Zhu, J. Hu, X. D. Fan, J. Yang, B. Liang, X. F. Zhu, J. C. Cheng, Y. F. Zhu, J. Hu, X. D. Fan, J. Yang, B. Liang, X. F. Zhu, J. C. Cheng, *Nat. Commun.* **2018**, *9*, 1632.
[8] C. Faure, O. Richoux, S. Felix, V. Pagneux, *Appl. Phys. Lett.* **2016**, *108*, 064103.
[9] H. Esfahlani, S. Karkar, H. Lissek, J. R. Mosig, *PRL B* **2016**, *94*, 014302.
[10] Y. H. Yang, H. P. Wang, F. X. Yu, Z. W. Xu, H. S. Chen, *Sci. Rep.* **2016**, *6*, 20219.
[11] E. Dong, P. Cao, J. Zhang, S. Zhang, N. X. Fang, Y. Zhang, *Natl Sci Rev* **2023**, *10*, nwac246.
[12] Z. Tian, C. Shen, J. Li, E. Reit, Y. Gu, H. Fu, S. A. Cummer, T. J. Huang, P. A. Metasurfaces, *Adv. Funct. Mater.* **2019**, *29*, 1808489.
[13] Y. B. Xie, W. Q. Wang, H. Y. Chen, A. Konneker, B. I. Popa, S. A. Cummer, *Nat. Commun.* **2014**, *5*, 5553.
[14] K. Tang, C. Y. Qiu, M. Z. Ke, J. Y. Lu, Y. T. Ye, Z. Y. Liu, *Sci. Rep.* **2014**, *4*, 6517.
[15] J. Mei, Y. Wu, *New J Phys* **2014**, *16*, 123007.
[16] S. Koo, C. Cho, J. H. Jeong, N. Park, *Nat. Commun.* **2016**, *7*, 13012.
[17] G. Memoli, M. Caleap, M. Asakawa, D. R. Sahoo, B. W. Drinkwater, S. Subramanian, *Nat. Commun.* **2017**, *8*, 14608.
[18] J. F. Li, C. Shen, A. Diaz-Rubio, S. A. Tretyakov, S. A. Cummer, *Nat. Commun.* **2018**, *9*, 1342.
[19] C. Li, M. Ke, Y. Ye, S. Xu, C. Qiu, Z. Liu, *Appl. Phys. Lett.* **2014**, *105*, 104301.
[20] E. Bok, J. J. Park, H. Choi, C. K. Han, O. B. Wright, S. H. Lee, *Phys Rev Lett* **2018**, *120*, 044302.
[21] G. Feng, F. Li, W. Xuea, K. Sun, H. Yang, Q. Pan, Y. Cao, *Appl. Surf. Sci.* **2019**, *463*, 741.
[22] Y. Liu, J. Chen, W. Xue, D. Zhu, W. Liu, Y. Cao, *Appl. Acoust.* **2021**, *180*, 108139.
[23] A. M. Kietzig, S. G. Hatzikiriakos, P. Englezos, P. S. M. Surfaces, *Langmuir.* **2009**, *25*, 4821.
[24] A. M. Kietzig, M. N. Mirvakili, S. Kamal, P. Englezos, S. G. Hatzikiriakos, *J. Adhes. Sci. Technol.* **2012**, *25*, 2789.
[25] A. Volpe, C. Gaudiuso, L. Di Venere, F. Licciulli, F. Giordano, A. Ancona, *Coatings* **2020**, *10*, 587.
[26] J. T. Cardoso, A. I. Aguilar-Morales, S. Alamri, D. Huerta-Murillo, F. Cordovilla, A. F. Lasagni, J. L. Ocaña, *Opt Lasers Eng* **2018**, *111*, 193.
[27] A. Volpe, S. Covella, C. Gaudiuso, A. Ancona, *Coatings* **2021**, *11*, 369.
[28] C. V. Ngo, D. M. Chun, *Appl. Surf. Sci.* **2017**,*409*, 232.
[29] G. Giannuzzi, C. Gaudiuso, R. Di Mundo, L. Mirenghi, F. Fraggelakis, R. Kling, P. M. Lugarà, A. Ancona, *Appl. Surf. Sci.* **2019**, *494*, 1055.
[30] A. De Bruijn, *Acta. Acust. Acust.* **1967**, *18*, 123
[31] X. Sheng, J. Zhang, *Colloids Surf., A* **2011**, *377*, 374
[32] F. Liu, S. Peng, H. Jia, M. Ke, Z. Liu, *Appl. Phys. Lett.* **2009**, *94*, 225.
[33] H. X. Sun, S. Y. Zhang, X. J. Shui, *Appl. Phys. Lett.* **2012**, *100*, 104301.